Lagrangian transport across the upper Arctic waters in the Canadian Basin

F. Balibrea-Iniesta[1], J. Xie[2], V. J. García-Garrido[1,3], L. Bertino[2],
A. M. Mancho[1], S. Wiggins[4]
[1]Instituto de Ciencias Matemáticas, CSIC-UAM-UC3M-UCM, 28049, Madrid, Spain.
[2]Nansen Environmental and Remote Sensing Center, Bergen, Norway.
[3]U.D. Matemáticas, Universidad de Alcalá, 28871, Alcalá de Henares, Spain.
[4]School of Mathematics, University of Bristol. Bristol BS8 1TW, UK.

The goal of this paper is to study transport, from a Lagrangian perspective, across selected circulation patterns in the upper Arctic Ocean waters. To this end, we apply the methodology of Lagrangian descriptors, using the function M, to the velocity field dataset provided by the Copernicus Marine Environment Monitoring Service. We focus our analysis on the Arctic region in the halocline (top 30 meters depth), which is based on particular events occurring over the 2012-2016 time period. The advantage of the Lagrangian descriptor is that it highlights large-scale persistent dynamical structures related to mathematical objects known as invariant manifolds, which determine fluid transport and mixing processes. These geometrical flow structures play a crucial role in the evolution of the freshwater content observed over the Arctic basin. In this work, we identify these dynamical structures in the Beaufort Sea and show how they mediate transport processes according to a clockwise circulating pattern, related to the Beaufort Gyre (BG). Additionally, this approach highlights the Transpolar Drift Stream (TDS) as a transport barrier which maintains the salinity gradient between the Canadian basin and the Atlantic waters. Our approach also illustrates the variability of the intensity of the TDS during the analyzed period and identifies secondary currents that feed it.

Key Words: Lagrangian transport, dynamical systems tools, hyperbolic trajectory, invariant manifolds, Lagrangian descriptors, data assimilation.

Received ...

1. Introduction

The Arctic Ocean is one of the regions most sensitive to climate change. This phenomenon, known as "Arctic amplification" (Cohen et al. 2014), is manifested by dramatic changes of the Arctic sea ice cover, including the reduction of ice extent and the thinning of the ice (Krishfield et al. 2014). The enhanced melting of sea ice contributes to the freshening of the surface Arctic waters (Morison et al. 2012), together with an intensification of the hydrological cycle. The Arctic Ocean is connected with the major ocean basins through four geographic features: the Bering Strait, the Canadian Archipelago, the Fram Strait and the Barents Sea. Most of the water exchanges are concentrated in the Fram Strait and the Barents Sea, where the saline Atlantic waters enter (of positive temperature and high salinity close to 35 psu). The connection to the fresher Pacific Ocean is more limited by the narrow Bering Strait but still constitutes a large source of freshwater to the Arctic (Carmack et al. 2016), which eventually exits the basin in equal parts through the nearby Canadian Archipelago and across the Arctic through the Fram Strait (Tsubouchi et al. 2017). The ocean surface circulation is to a large extent driven by the sea ice drift, whose main classical time-averaged features are the anticyclonic Beaufort Gyre and the Transpolar Drift Stream (TDS), which is able to transport ice parcels frozen on the Siberian Shelves to the Fram Strait within 2 to 4 years

(L.A. 2001) and causes about 10% of the ice volume to exit through the Fram Strait every year (Rampal et al. 2011). As an ocean current feature, the TDS transports a share of the fresh water from the Siberian shelves across the central Arctic to the Fram Strait. In ice-free areas, the surface currents are more influenced by the winds. Another strong effect in the Arctic circulation is the topographic steering of the ocean currents (Holloway et al. 2011). The resulting surface circulation is illustrated in Figure 1. The Arctic Ocean is also characterized by its positive precipitation-evaporation balance. The amount of river run-off (the main source of freshwater) and snow/rain widely overcomes the total evaporation of water in the Arctic, which makes the surface freshwater thus maintain the Arctic upper-ocean stratification. The Arctic water masses of interest to our study are thus within the Arctic Mixed Layer, for which typical depths vary in the Western Arctic from 8 m in summer to 30 m in winter (Peralta-Ferriz and Woodgate 2015): the warm and fresh Pacific Summer Waters (of temperature between -1 deg C and 0.5 deg C, whereas the Pacific Winter Water can be found down to 150 m depths (Dmitrenko et al. 2016)), the colder and relatively more saline resident Beaufort Sea Water and Upper Halocline Waters of salinity lower than 31.5 psu and near freezing point temperature found on either sides of the TDS. The Arctic Mixed Layer is isolated from the Atlantic water by the Upper and Lower Halocline Waters, although the gradual erosion of the halocline by several factors has been observed in a few locations in the Arctic (Polyakov et al. 2017).

The largest freshwater storage in the Arctic Ocean resides in the Beaufort Gyre, an anticyclonic gyre in the upper 400 meters of the Canadian Basin (Aagaard and Carmack 1989; Proshutinsky et al. 2009). The latter review indicates that the Beaufort Gyre receives freshwater from the Arctic shelves by Ekman pumping during the winters when strong winds enhance the anticyclonic ocean and sea ice circulation. Sea ice meltwater contributes to the freshwater storage in summer. Two-dimensional model simulations indicate that during the years 2004-2010 freshwater pathways tend to lead to the Beaufort Gyre but highlight a significant interannual variability: for example in the year 2010 when freshwater spread towards the Eurasian Basin due to anomalous wind patterns, which caused a shift of the Transpolar Drift Stream to the Switchyard region, north of Greenland (Timmermans et al. 2011). Important features of the Beaufort Sea circulation include the inflow of warm and fresh Pacific waters from the Alaskan Coastal Current close to the coast (Spall 2007), after a residence time reported between six months (Panteleev et al. 2010) and one year (Spall 2007) in the Chukchi Sea , its partial retroflection into the Chukchi Sea (Pickart et al. 2017), the aforementioned Beaufort Gyre in deeper waters, the freshwater discharge from the Mackenzie river and an intense mesoscale eddy activity (Watanabe 2011), forming in the Summer between Barrow Canyon and the Beaufort shelf break.

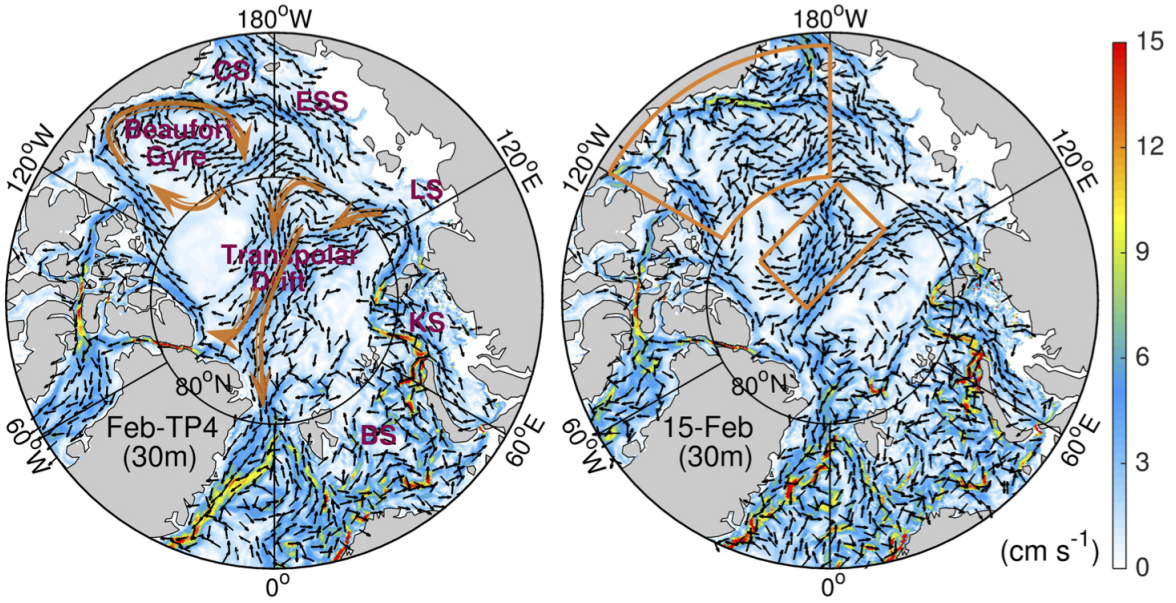

Figure 1. a) The Arctic February mean circulation near the surface during the period 2012-2016 obtained from the TOPAZ reanalysis. In red are the names and initials of the major Arctic ocean features. The orange solid arrows represent the dominant current systems; b) the Arctic ocean current circulation on the 15th February 2013 at the 30 m depth layer also from the TOPAZ reanalysis product. Orange solid contours surround the areas where this study is focused.The current speeds are denoted by shading, and the velocity vectors are shown at every 6 grid nodes, except where the mean velocity is below 1 cm/s.

In this article we explore transport across selected upper ocean circulation patterns as revealed by a regional model reanalysis (Xie et al. 2017). We examine those in the period from 2012 to 2016 by means of Lagrangian techniques and identify the dynamical barriers responsible for the freshwater storage in the Canadian Basin. Our focus is on two specific features of those visible in Fig. 1a): the Beaufort Gyre and the Transpolar Drift. Fig. 1b) surrounds in blue contours the areas under study. Typically major circulation currents in the Arctic Ocean have been described from a climatological perspective that considers averaged velocity fields over a long period, and therefore the characterization has been restricted to the Eulerian point of view. Such a perspective for the surface circulation patterns in the Arctic is summarized in Fig. 1a). This work provides a complementary perspective to the climatological Eulerian description by examining horizontal Lagrangian transport across the two specific features aforementioned. Our transport analysis is based on daily velocity data sets produced by an accurate numerical simulation of the Arctic Ocean (Xie et al. 2017). Figure 1b) displays Arctic currents on the specific date of 15th February 2013 obtained from these simulations at the depth of 30m, showing that the identified features of interest in the daily basis are not so clearly distinguished as in Figure 1a). The perspective taken in our study is not on analyzing correlations between the fields of the reanalysis product and the observed physical magnitudes, but

just on analyzing the transport that occurs in the reanalysis velocity fields. Arctic currents, in particular in the interior regions of the Beaufort Sea, present typical velocities which are much slower to those found in other oceans. In these regions particles may take from months to years to navigate significant distances. Although transport timescales in the areas in which our study is focused are longer than in other areas, questions relative to the qualitative and quantitative description of fluid transport and horizontal mixing issues remain the same. For example, even in apparently simple velocity fields, nearby particles can evolve following completely different paths (i.e. the ocean currents are subject to chaotic dynamics and are thus sensitive to the initial conditions of fluid parcels). In order to address this difficulty, many ideas based on Poincaré's works on dynamical systems theory have been proposed in the past decades, see, e.g. (Aref 1984; Ottino 1989; Wiggins and Ottino 2004). This paradigm, known as the dynamical systems approach to Lagrangian transport seeks to discover geometrical flow structures that divide the ocean (phase space) into distinct regions corresponding to trajectories with qualitatively different dynamical behaviors. These distinguished material fluid structures are relevant because they act as transport barriers that fluid particles cannot cross, becoming the principal agents that mediate transport and mixing processes between different flow regions. In this way, they govern the evolution of passive tracers. In a first approach, to be explored throughout this manuscript, heat, salt and carbon dioxide and also potential contaminants produced by human exploitation of Arctic resources can be represented as passive tracers *. All these elements play a key role in the present and future of the Arctic Ocean ecosystem. In particular, the Lagrangian tools that we have used in this article identify well the Transpolar Drift and revisit the paradigm of the Beaufort Gyre from the perspective supplied by the analysis of daily data. We find that in this analysis dynamical systems concepts such as invariant manifolds are detected as present in the Arctic Ocean, and confirm that they play a key role in governing clockwise transport in the Beaufort Sea.

The article is organized as follows. Section 2 introduces the datasets, the Lagrangian tools and the dynamical systems concepts used in this work. Section 3 comes back to this analysis by describing these features from the Lagrangian point of view in the Arctic ocean. Finally, in Section 4 we present the conclusions.

2. Datasets and dynamical systems tools

2.1. The CMEMS dataset

In order to describe the Arctic Ocean circulation patterns, we use the velocity and salinity fields distributed by the Copernicus Marine Environment Monitoring System (CMEMS). The product called "Arctic Ocean Physics Analysis and Forecast" is available at *http://marine.copernicus.eu/*. It is based on the TOPAZ4 ice-ocean prediction system, which is an operational real-time ocean monitoring and forecasting system covering the North Atlantic and Arctic Oceans with a resolution of 12.5 km (Sakov et al. 2012; Melsom et al. 2015). TOPAZ4 is based on the HYbrid Coordinate Ocean Model (HYCOM Bleck (2002)), using 28 hybrid z-isopycnic layers and mixed layer processes by the K-Profile Parameter model (KPP, Large et al. (1994)). HYCOM is coupled to a sea ice model with an Elastic-Visco-Plastic rheology (Hunke and Dukowicz 1997) and simple thermodynamics. The model domain extends to the Tropical Atlantic, but is cut at the shallow Bering Strait where a barotropic water flux is imposed, for which seasonal variations are following the observations from Woodgate et al. (2005), the mean flow is 0.8 Sv, the minimum is 0.4 Sv in summer and the maximum 1.3 Sv in winter. The water mass properties of the incoming Pacific Waters are relaxed to climatological values from the World Ocean Atlas 2013 (WOA13). The wind forcing is from the ECMWF ERA-Interim reanalysis (Dee et al. 2011) and river fluxes are obtained all around the Arctic from the ERA-Interim land runoffs, channeled into the Total Runoff Integrated Pathways (TRIP) model at 0.5 degree (Oki and Sud 1998). TOPAZ4 uses the Ensemble Kalman Filter (EnKF) with 100 dynamical members for assimilating satellite ocean and sea ice observations as well as in situ ocean profiles, including those from Ice-Tethered Profilers (ITPs). The TOPAZ4 production cycle is run on a weekly basis, starting with a data assimilation step, which causes a temporal discontinuity in the time series. The data assimilation is performed locally with radius of influence of 90 km (Sakov et al. 2012). The assimilation is followed by a one-week 100-members ensemble simulation run, from which the ensemble mean provides a best estimate. The assimilation updates all prognostic variables in HYCOM: the water mass properties, the current velocities and the isopycnic layer thicknesses. In the isopycnic domain of the model, this update ensures the conservation of linear relationships, for example the geostrophic balance (Evensen 2003). The update of temperature and salinity at a given density also ensures the stability of the water column after analysis. However, in the upper z-level domain, no such constraints apply and the assimilation imbalances may be more pronounced. The TOPAZ4 reanalysis covers the years 1992-2016 and is updated on a yearly basis. Due to changes in the reanalysis settings (Xie et al. 2017), only the years previous to 2016 are considered for the present study. The comparison against assimilated ITPs in (Xie et al. 2017, their Figure 9) (Xie et al. 2017) shows that the cold halocline lies as expected above the core of the Atlantic Water, although the AW temperature is too cold in the central Arctic region. Otherwise the near surface properties are on average more accurate than those of the WOA13 climatology. The TOPAZ4 mixed layer depth in the Western Arctic is about 15 m in Summer and 30 m in Winter (Uotila et al. 2018, their Figures S5 and S6) (Uotila et al. 2018), which agrees well with observations (Peralta-Ferriz and Woodgate 2015) and other model reanalysis (Uotila et al. 2018). The assimilation system constrains the modeled sea ice edge within 50 km from the observed ice edge and the sea ice drift patterns are respected as well, although the centroid of the Beaufort Gyre is however shifted 200 km too far off the shelf into the Canadian Basin compared to satellite data (Xie et al. 2017). The ocean currents are shifted similarly below the ice, but seem better located with higher horizontal ocean model resolution (not shown).

The velocity and salinity data are provided over 12 depth levels, varying from 5 m to 3000 m, from 2012 to 2016 as daily averages. Vertical interpolation has been used for convenience to avoid handling the transitions between isopycnic and z-level coordinates and a fixed depth of 30 m has been selected as most representative of the Upper Halocline Waters, as

*Even though heat and salt are strictly speaking active tracers.

will be shown below. At each vertical level, the fields have a horizontal spatial resolution of 12.5 km (a grid of 881×609 geophysical points expressed in polar stereographic projection coordinates (x, y)), covering the North Atlantic, the Arctic Ocean and other adjacent seas. The use of this projection is convenient to bypass the singularity that arises at the North Pole when working with longitude/latitude coordinates.

2.2. The Dynamical Systems Approach

In order to understand transport and mixing processes and the circulation patterns across the Arctic Ocean within the halocline level, we examine particle evolutions using a purely advective approach. We assume that particle motion is approximately quasi-horizontal, and thus motions are restricted to a 2D plane. More specifically our study is focused in the layer at 30m depth. The 2D approach for the study of transport in oceanic flows has many previous successful examples (Branicki et al. 2011; Branicki and Kirwan Jr. 2010; Mendoza et al. 2014). This approach takes advantage of the fact that particles move on isopycnals and typically these are close to horizontal layers in the surface. A similar approach is frequently taken in studies in the stratosphere in which particles move on isentropic surfaces (de la Cámara et al. 2009, 2013). A fully 3D study of transport processes in these later flows is reported in (Curbelo et al. 2017). This study confirms that in the stratosphere and upper troposphere full 3D Lagrangian structures are curtain like structures well approximated as stacks, weakly varying along the vertical coordinate, of the evolving stable and unstable manifolds calculated on 2D surfaces. In particular (Curbelo et al. 2017) has shown that typical of this curtain like structures is the vertical extension of the hyperbolic trajectories throughout the vertical coordinate, forming a mathematical object called a Normally Hyperbolic Invariant Manifold (NHIM) ((Wiggins 1994; Mezic and Wiggins 1994)). We will confirm that this description fits well in our study, even for the regions in which vertical motions may be more important. In particular, we show that vertical motions in the considered data are not important enough as to destroy this structure. This is consistent with the fact that for typical upwelling events described for the Alaskan Beaufort Sea (see (Lin et al. 2017)), the reported vertical motions at about 50 m depths are of the order of 5 meters per day (0.006 cm/s), which is small compared to horizontal currents which are about 20 cm/s. More details on this discussion will be given later.

Under these assumptions, fluid particles follow trajectories $\mathbf{x}(t) = (x(t), y(t))$ that evolve according to the dynamical system:

$$\frac{d\mathbf{x}}{dt} = \mathbf{v}(\mathbf{x}(t), t) \ , \tag{1}$$

where $\mathbf{v} = (v_x, v_y)$ are the ocean velocity components along the (x, y) polar stereographic projection coordinates (projection parameters given in the metadata). The results discussed later in this article, require the integration of particle trajectories in Eq. (1), where the velocity field $\mathbf{v}$, is provided on a discrete grid. To obtain a continuous description, the velocity field is interpolated with a cubic scheme both in space in time, and then the integration of particle trajectories is performed by means of a Cash-Karp Runge-Kutta scheme with a fixed integration time step.

Among the geometrical features that divide the ocean surface into sectors with qualitatively different dynamical behaviors, of particular interest are hyperbolic trajectories ((Ide et al. 2002; Jones and Winkler 2002; Wiggins 2005; Mancho et al. 2004)), which highlight regions in the fluid characterized by high expansion and contraction rates. Figure 2a) illustrates how blobs in the neighborhood of these trajectories evolve from time t_0 to t_1, contracting along the so-called stable direction (stable manifold) and stretching along the unstable direction (unstable manifold). Thus particles in the stable and unstable directions of the hyperbolic trajectory evolve, respectively, by approaching or moving away from the hyperbolic trajectory. A special configuration of the hyperbolic trajectory, which is of particular interest for this work, is that illustrated in Figure 2b). It consist of a hyperbolic point attached to the coast in which the stable manifold is aligned with the shoreline, but the unstable manifold is transversal to it. This configuration is called a detachment point as on it particles evolve separating from the coast and penetrating into the waters, as evidenced by the blobs at successive times in Figure 2b). In general, given any configuration in Fig. 2, if the time interval between t_0 and t_1 is long enough, the blob particles align along a — possibly complex — curve, the unstable manifold, which is an attracting material curve: advected particles remain close to it for a sufficiently long time. Similarly, but going backwards in time, blob particles align along a repelling material curve: the stable manifold, which also may be very complex. Complex stable and unstable manifolds are generated by the folding caused by the nonlinearities present in the velocity field, beyond the neighbourhood of the saddle, in which stretching is the dominant feature. Stretching and folding of material lines are the essential ingredients to produce chaos, as exemplified by the so-called "Smale horseshoe map", considered the "heart" of chaotic dynamics (see Smale (1967, 1980)).

Apart from hyperbolic trajectories, other types of dynamical flow structures exist, in which particles tend to stay together, coherently, without dispersing. In 2D flows these include eddies or jets, which act as dynamical barriers that trap fluid in their interiors ((Mancho et al. 2006; Samelson and Wiggins 2006)). Figure 3 shows the evolution of blobs in this type of flow. Vortices keep fluid parcels inside them and jets transport them with small distortion. Eventually all possible complex particle evolutions in time dependent 2D flows, such as the ocean, are then a result of transitions between these elementary features (vortices, jets and hyperbolic trajectories and their stable and unstable manifolds) and their nonlinear interactions. The three aforementioned features cover exhaustively all possibilities in typical 2-dimensional ocean flows.

Several Lagrangian methods have been developed in the literature to reveal a geometrical template from time dependent velocity fields, a template formed by the stable and unstable manifolds of hyperbolic trajectories and other coherent structures in flows with aperiodic time dependence. For instance, manifolds have been approximated by computing ridges of fields, such as Finite Size Lyapunov Exponents (FSLE) (Aurell et al. 1997) and Finite Time Lyapunov Exponents (FTLE) (M. 1989; Shadden et al. 2005). Distinguished Hyperbolic Trajectories (DHT) (Ide et al. 2002; Ju et al. 2003; Madrid and Mancho 2009) and their stable and unstable manifolds (Mancho et al. 2004, 2006; Mendoza and Mancho 2012) also provide another perspective. In the present work we use the Lagrangian Descriptors (LDs), in particular those depicted by the

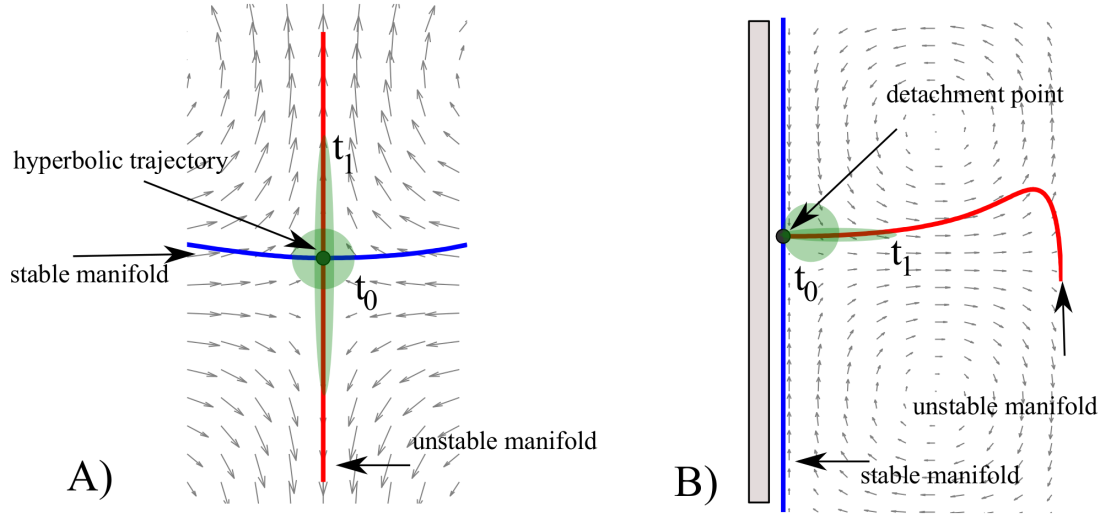

Figure 2. Evolution of blobs from t_0 to t_1 in the neighbourhood of two hyperbolic trajectories in different dispositions: a) in the interior of the flow; b) along the coastline in a detachment configuration.

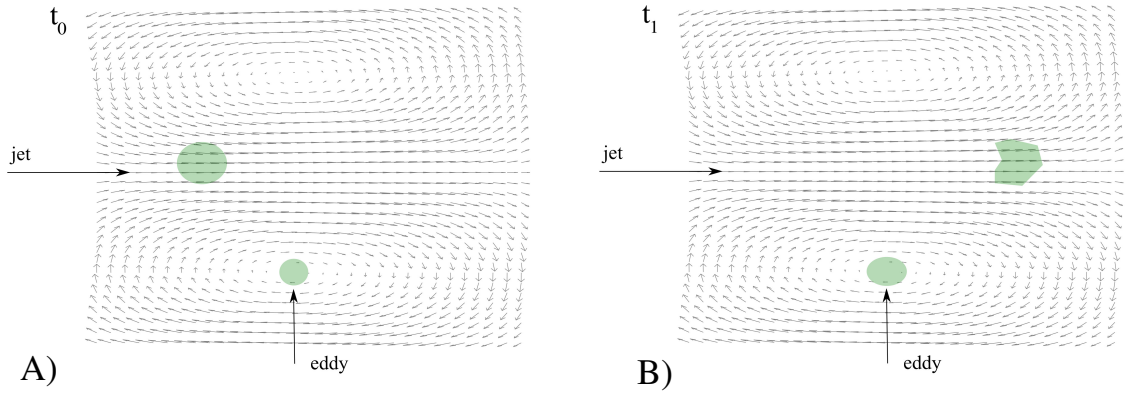

Figure 3. Evolution of a blob in the interior of a vortex and within a jet from t_0 (a) to t_1 (b).

function M (Mendoza and Mancho 2010; Mancho et al. 2013), defined as follows:

$$M(\mathbf{x}_0, t_0, \tau) = \int_{t_0-\tau}^{t_0+\tau} ||\mathbf{v}(\mathbf{x}(t), t)|| \, dt \, , \tag{2}$$

where $||\cdot||$ represents the Euclidean norm. At a given time t_0, the function M measures the arclength of a particle trajectory starting from $\mathbf{x}(t_0) = \mathbf{x}_0$ as it evolves forwards and backwards in time for a period $\tau > 0$. In order to evaluate M we need to solve Eq. (1) in order to compute the particle trajectories. To do so, given an initial time t_0, a value for τ is chosen and a grid of initial conditions $\mathbf{x}_0$ is chosen in the region of interest. The function M depends on τ. For small τ it provides a smooth pattern in which larger M values are related to fluid regions of highest speed (such as jets), while small M values denote calmer regions. At larger τ values, this function develops singular features aligned with invariant stable and unstable manifolds. A representation of M evaluated for $\tau = 10, 30, 50$ and 300 days is presented in Figure 4. At $\tau = 300$ the displayed manifold structure is richer than that visible at lower τ values. This is related to the fact that at longer times the particle history is more complex than that possible for shorter times, and therefore the successive images displayed in Figure 4 show an increment of the Lagrangian historical background, but there is no contradiction among them. Panel d) emphasizes blue and red curves aligned with stable and unstable manifolds. These curves are material barriers that cannot be crossed by fluid parcels, and this is the case for all the singular lines distinguishable from panel b) onwards. Panel d) also displays, with a white dot, a hyperbolic point in which invariant manifolds cross. This is a very relevant hyperbolic point for which we will describe further results in the next section. The τ value is selected according to the information of interest for a particular velocity field. Since the Arctic currents are slow in the areas of interest, such as the interior of the Beaufort Gyre, the integration period τ must be long enough to reveal the relevant Lagrangian structures in their interior. Additional hyperbolic trajectories are found at the crossing points of singular features. Fig. 5 displays the evaluation of M between the 1st of April and the 1st July 2013 over the Beaufort Sea, using also $\tau = 300$ days. In Fig. 5 a) the blue and red curves are aligned, respectively, with the stable and unstable manifolds, which intersect at hyperbolic trajectories. All

the points in the intersecting lines are hyperbolic, however we just test one of them with four illustrative blobs, which are placed over the singular features aligned with manifolds. The evolution of both blobs and the manifolds is shown for the 1st May, 1st June and 1st of July 2013 in Figs. 5 b), c) and d), respectively, confirming the hyperbolic character of the crossing lines as the blobs stretch and contract along the unstable and stable manifolds. The fact that particles remain on the sharp boundaries of the pattern, confirm the invariant character of these features. The velocity field is overlapped in the figure, confirming that the long term behaviour displayed by the M function is not obvious from Eulerian fields. One drawback of using long periods τ in regional models could be that the trajectories might hit the model boundary. In the above example, the Pacific Waters only have a residence time between 6 months and one year in the Chukchi Sea, so a part of the particles may have hit the TOPAZ4 model boundary in the Bering Strait and may seem younger than it actually is. This limitation does otherwise not impair much the dynamical interpretation of the features of the M function. This is illustrated in Fig. 4 with the use of an increasing τ, which shows a consistent M pattern throughout all the taken τ values, and in the consistent interpretation of the lines visible in Fig. 5, which have been obtained for $\tau = 300$ days, as material lines made in terms of blobs.

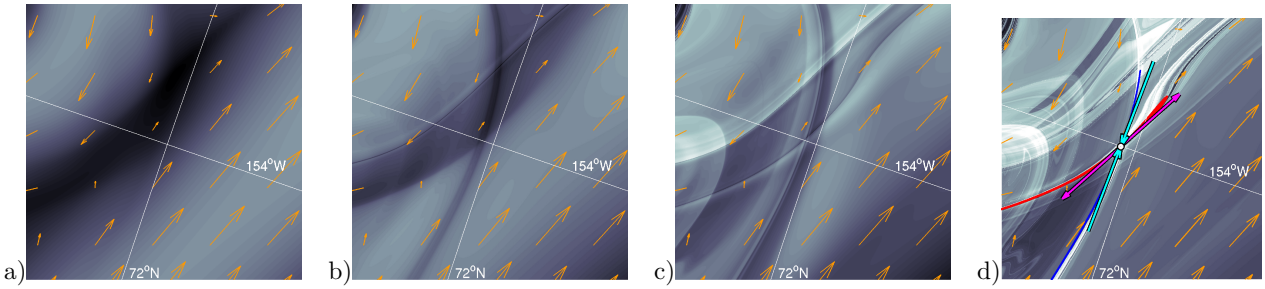

Figure 4. Evaluation of M for increasing τ values on the 15th October 2013. a) $\tau = 10$; b) $\tau = 30$; c) $\tau = 50$; d) $\tau = 300$. For $\tau = 300$ a white dot marks the position of a hyperbolic trajectory. Magenta and cyan arrows show, respectively, the unstable and stable directions with their associated manifolds in the red and blue color respectively.

Figure 6 shows that the M function also has the capability of highlighting jets present in the fluid (see (Mancho et al. 2013; de la Cámara et al. 2009, 2013; Curbelo et al. 2017)). In this particular case, the TDS is clearly visible through the whiter color, which highlights the parts of the jet with the highest speeds. This figure shows the evolution of a blob between the 15th August 2013 and the 1st January 2014. The blob evolves within the jet with low distortion, if compared to the filamentation experienced near a hyperbolic point, confirming the schematic representation of figure 3. Typically, vortex- or jet-like structures are mathematically related for periodic domains to one dimensional tori (1-tori) or two dimensional tori (2-tori). In continuous time systems 1-tori are periodic trajectories. Periodic trajectories are localized and are characterized by a single frequency and they trap regions of fluid. 2-tori are characterized by two frequencies whose ratio is not a rational number (they are said to be incommensurate). While such trajectories are not closed (like periodic orbits) they trace out a two dimensional torus. Such a flow structure traps regions of fluid in the same way as periodic orbits. There exist formal results linking contour lines of the time average of M with tori-like invariant sets (Lopesino et al. 2017). In this manner, contour lines of converged averages of M highlight invariant tori. In the Arctic case, however, the average of M does not converge as the flow is aperiodic and thus contours of M do not strictly represent invariant sets.

3. Lagrangian analysis results

We discuss next the results of our Lagrangian analysis by means of the function M over selected upper circulation Arctic features within the Canadian basin: the Beaufort Sea and the Transpolar Drift. We study transport processes on 2D velocity

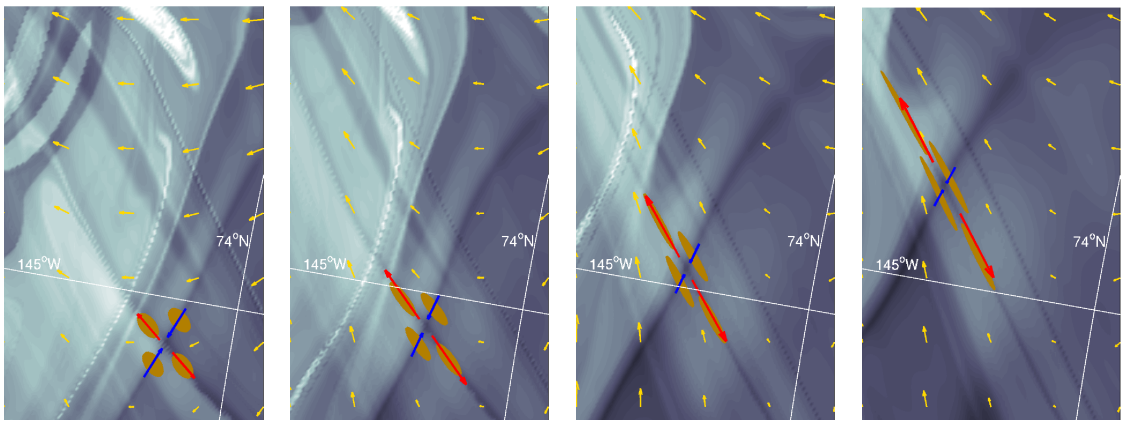

a) 1st April 2013 **b)** 1st May 2013 **c)** 1st June 2013 **d)** 1st July 2013

Figure 5. Evolution of the structures arising over the Beaufort Sea area as sharp changes of the values of M for an integration time of $\tau = 300$ days. Overlapped are the velocity fields. Panel **a)** depicts four blobs of fluid particles aligned with the stable and unstable manifolds of a hyperbolic trajectory located in the Beaufort Sea on the 1st of April 2013. The directions of the stable and unstable manifolds of the hyperbolic trajectory are marked in blue and red color respectively. **b)**, **c)** and **d)** show the evolution of the four blobs of particles and of the surrounding Lagrangian structures on different dates.

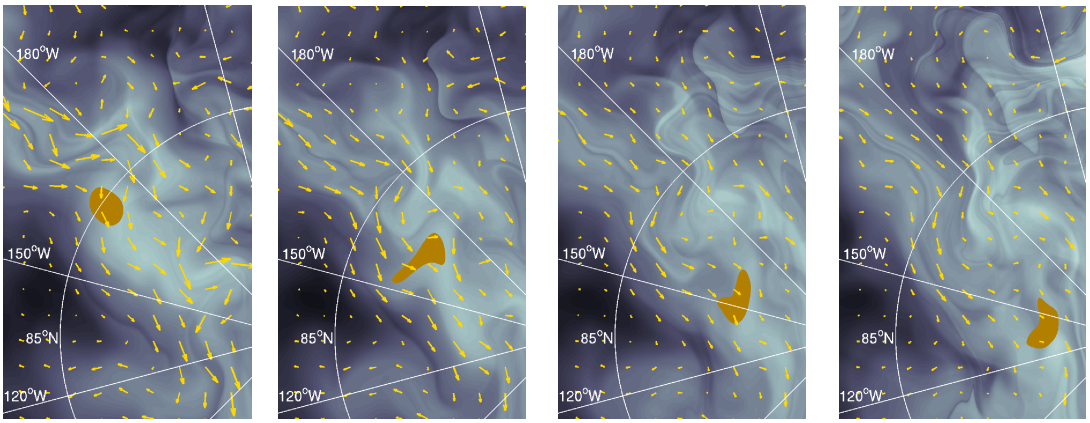

Figure 6. Identification of the Transpolar Drift Stream (TDS) in the Arctic Ocean by means of function M evaluated with $\tau = 300$ days. Overlapped are the velocity fields. On the 15th of August 2013 (picture **a)**) a blob of water particles is placed on the jet. The evolution of the fluid blob and the Lagrangian structures based on function M are shown in panels **b)**, **c)** and **d)** on different dates.

fields produced by CMEMS at 30 m depth (within the halocline), so that the ocean currents do not bear the marks of the sea ice motions on the surface, and also discuss on the suitability for our 2D approach.

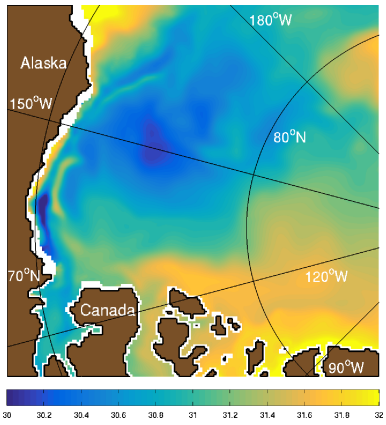

Figure 7. Representation of the salinity at 30 m depth on the 1st April 2013. The colorbar varies from 30 to 32 psu.

We start our discussion by considering transport in the Beaufort Gyre. This element has been characterized as a wind-driven current which accumulates the largest amount of freshwater in the Arctic Ocean. Figure 7 confirms the presence of a salinity anomaly in the Beaufort Sea in April 2013 as provided by the analyzed data set. This anomaly is maintained throughout the year although it experiences slight fluctuations. Next we provide dynamical insights into the presence of this anomaly, in particular to the salinity front, transversal to the Alaska coast, that retains slightly saltier (31 psu) Pacific Waters.

Figure 8 shows the evaluation of the function M for a selection of dates from October to December 2013 in an area of the Beaufort Sea. The figure highlights with a white dot the aforementioned hyperbolic point displayed in Figure 4 jointly with its stable (blue) and unstable (red) manifolds. The red and blue curves are depicted to emphasize the visualization of the stable and unstable manifolds, but these are already visible from the contours of the function M in the delicate sinuous lines that appear at the background. These curves highlight the dynamical barriers governing the transport processes. A rule of thumb for making the right interpretation for which lines correspond to stable and which ones to the unstable manifolds is that stable manifolds never cross stable manifolds (they always appear nested) and similarly occurs with the unstable manifolds. As a result crossing lines always correspond to manifolds with different stability.

The fact that the stable manifold is aligned with the coast and near to it, indicates that this hyperbolic trajectory has a configuration close to a detachment point, similar to that schematically represented in Figure 2 b), which is related to the phenomena of flow separation. Indeed, backwards integrations of particles placed in the neighborhood of the hyperbolic trajectory on the 1st of December (in blue) are displayed in Fig. 8 a)-e). On the 1st of October particles were spread along the stable manifold of this hyperbolic trajectory and its alignment with the coast is confirmed. Analogously, forward integrations of particles placed in the neighborhood of the hyperbolic point on the 1st of October are displayed in Fig. 8 e) for the 1st of December, confirming that the unstable manifold is transversal to the coast. These simulations confirm the major role played by this hyperbolic trajectory, since its manifolds extend for a few weeks in the forward and backwards time integration over large Arctic areas. This saddle is placed close to an Arctic area, the Barrow Canyon, for which upwelling motions have been reported (Lin et al. 2017), thus the 2D approach taken for our description requires further verification. According to fully 3D Lagrangian studies in geophysical flows such as those reported in (Curbelo et al. 2017, 2018b), a class of 3D flows commonly occurring in this context possesses Lagrangian structures consisting of a stack of 2D Lagrangian structures. These type of structures are produced when vertical motions are small compared to the horizontal velocity components, which are the dominant ones. As explained before, this setting is consistent with velocity fields in

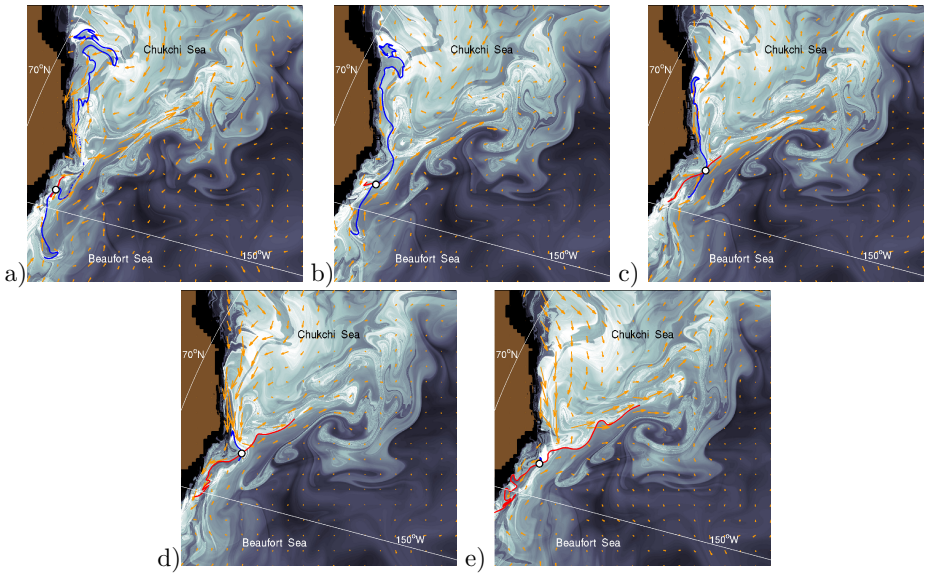

Figure 8. The configuration of a detachment point in the Arctic coastline, highlighted by means of the function M. The white dot highlights the hyperbolic trajectory and the red and blue curves denote, respectively, the unstable and stable manifolds. The velocity field is overlapped; a) 1st October 2013 b) 15th October 2013; c) 1st November 2013; d) 15th November 2013; e) 1st December 2013.

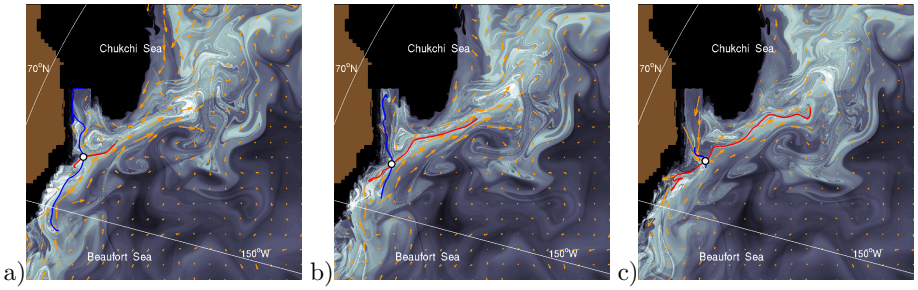

Figure 9. The detachment point at 50 m depth in the Arctic coastline, highlighted by means of the function M. The white dot highlights the hyperbolic trajectory and the red and blue curves stand respectively for the unstable and stable manifolds. The velocity field is overlapped; a) 15th October 2013; b) 1st November 2013; c) 15th November 2013

.

the area of study (see (Lin et al. 2017)). Horizontal velocities may vary with the vertical coordinate, and this would cause differences in the Lagrangian patterns at different levels, however the continuity of the horizontal velocities with respect to the vertical coordinate is responsible of the preservation of major Lagrangian features at different slices (see discussion of Section 2 in (Curbelo et al. 2017) for further details on the type of problem described). A typical feature in these flows is, for instance, the vertical extension of the hyperbolic trajectories throughout the vertical coordinate, forming a mathematical object called a Normally Hyperbolic Invariant Manifold (NHIM) (Wiggins (1994); Mezic and Wiggins (1994)). Figure 9 shows the calculation of the M function at a depth of 50 m. This figure confirms the vertical extension of the hyperbolic trajectory and of its stable and unstable manifold, verifying the curtain like structure of the Lagrangian structures, which at least in these depth ranges, are not destroyed by the vertical motions.

The hyperbolic point of figure 8, strictly speaking, is not in the coast, as it would be the case of detachment points. It is placed near the exit of Barrow Canyon, which channels the Pacific Waters from the Alaskan Coastal Current (Spall 2007). The hyperbolic trajectory is on a strong current or jet that Chukchi Sea waters do not cross and as described by Watanabe (2011), give rise to a cyclonic/anticyclonic eddy pair. From our dynamical systems perspective the unstable manifold of this hyperbolic trajectory conforms a barrier, and this barrier character is confirmed by the evolution of particle blobs at both sides, as visible in Figure 10. Figures 10 a), b), c) show the evolution of the blobs at selected dates while figures 10 d) and e) show the time evolution of the average of temperature and salinity within each blob and f) shows the Temperature-Salinity (TS) diagram for these time series. These diagrams confirm that the barrier is present for several months in the eddy pair (described as Type 1 eddies in Watanabe (2011)) and that after a period the waters eventually mix when the eddies dissipate. The time evolution of the water masses depicted in Figure 10, shows that the salinities in the blob within the Beaufort Sea experience, on the 1st of October 2013, a 0.3 psu gap. This is due to the aforementioned assimilation updates, which are not continuous in time. The time series shows that Pacific waters, i.e waters in the Chukchi Sea area, are initially warmer than the Beaufort Sea waters by 1.5 deg, but rapidly cool down during the Fall 2013. During that time, the melting and freezing of ice near surface water in the Beaufort Sea mostly changes its salinity but not its temperature. The freezing of surface water increases the salinity of the Pacific waters. From January 2014 onwards the water masses have almost the same properties and those remain stable until the end of the Summer 2014.

The animation S1 of the supplementary material confirms the moving character of the saddle just described. This movie shows the time evolution of the M function from the 1st of March 2013 until the 1st of March 2015 at 30m depth in a large Arctic area. The parameter τ in this calculation is also 300 days, and therefore the velocity data series required for computing M in the movie starts in 2012 and ends in 2016. In this animation the strongest whiter color in the M function

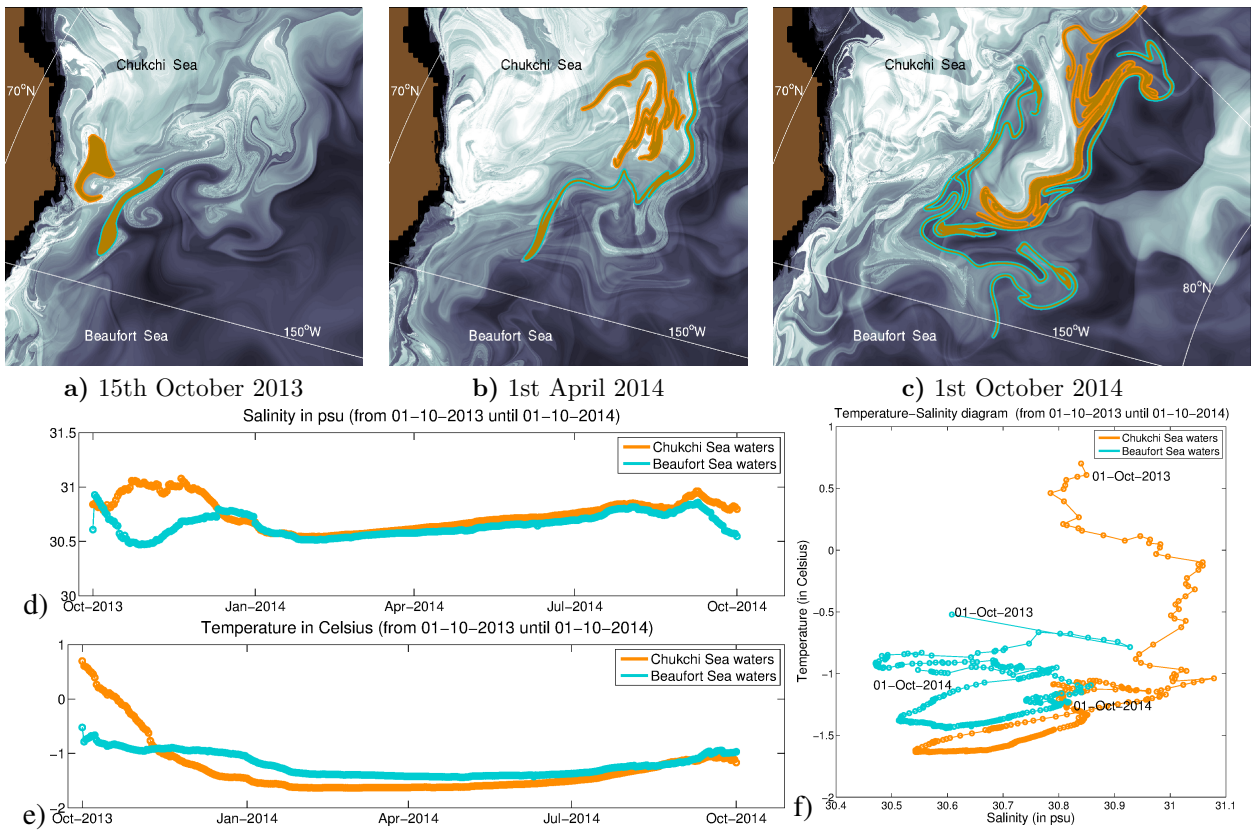

Figure 10. Evolution of Chuckchi and Beaufort Sea water masses. a) 15th October 2013; b) 1st April 2014; c) 1st October 2014; d) evolution of the salinity average within each blob; e) evolution of the temperature average within each blob; f) Temperature-Salinity diagram for the time series displayed in panels d) and e)

along the Canada and Alaska coasts highlights a strong current which oscillates in time, transporting fluid material from Canada towards Alaska. The movie additionally shows that this current finds an opposing current coming from Alaska, both resulting in a bent current which prevents direct water flux from the Bering Strait to the Beaufort Sea. This configuration forces the presence of the described detachment point close to Point Barrow, the moving saddle along the North America coast. The described hyperbolic trajectory is in qualitative agreement with the findings by Spall (2007) and Pickart et al. (2017) (see (Spall 2007; Pickart et al. 2017)) that report a branching of the currents coming from Chukchi Sea, to the west of the Beaufort Sea, from different perspectives based either in models (Spall 2007) or observations (Pickart et al. 2017).

We next discuss aspects on transport issues in the interior of Beaufort Sea, which are also visible from the movie S1. Figure 11 highlights selected days that support our discussion. In this figure, panel a) displays the function M calculated on the 1st of April 2013 for $\tau = 300$ days in this area. In this figure intricate lines that correspond to the pattern of the attracting and repelling material lines are emphasized with a cyan circle. A zoom of the manifold skeleton associated with the moving saddle is visible in panels b), c), and d). This figure shows a magnification of the complex patterns contained within the cyan circle of panel a). A yellow arrow in panel a) shows the position of stable manifolds which eventually transport material towards the major current, and the green arrow indicates penetration paths from the current to the Beaufort Sea according to the unstable manifolds. The set of three arrows compose a clockwise motion which we identify with the BG. The material surfaces just described are time dependent and their time evolution is visible in the movie S1. More specifically, panels b), c) and d) in Figure 11 show particles coloured green placed over visible unstable manifold features. Their time evolution from the 1st April 2013 to the 15 August 2013 confirm the motion according to the green arrow in panel a). They are located along a front, which is likely the edge of an anticyclonic Type 1 eddy (following Watanabe (2011). Yellow particles are placed just over visible stable manifold features, (Giles et al. 2012), which seems to collapse on the shelf break on the 1st August 2013. Finally, magenta particles are placed over visible stable and unstable manifold intersections which again evolve in agreement with the magenta arrow, providing evidence of a clockwise pattern. These are markers of transient small scale features, gradually aligning within the larger anticyclonic circulation feature. The movie confirms these findings on the transport routes as defined by the stable and unstable manifolds according to an anticyclonic (clockwise) gyre. In the transport description provided by the M function there is no sign of a big coherent gyre with a diameter of hundreds of kilometers as the climatological circulation displayed in Fig. 1 suggests. The transport analysis based on daily data confirms anticyclonic transport mediated by the stable and unstable manifolds of hyperbolic trajectories, but shows several complex features within the Beaufort Gyre. In particular in the pattern visible in figure 11a), zoomed in panel b), displaying crossing stable and unstable manifolds, is recognized a typical chaotic saddle structure. Chaotic saddles are important kinematic mechanisms that result in stretching and folding of fluid parcels, which results in fluid mixing (Ottino 1989, 1990). Specifically, in ocean contexts, d'Ovidio et al. (2004) have linked saddles to regions with mixing properties. In our particular case however, as waters in the area are rather homogeneous in their salinity content, the mixing activity may go unnoticed in this regard.

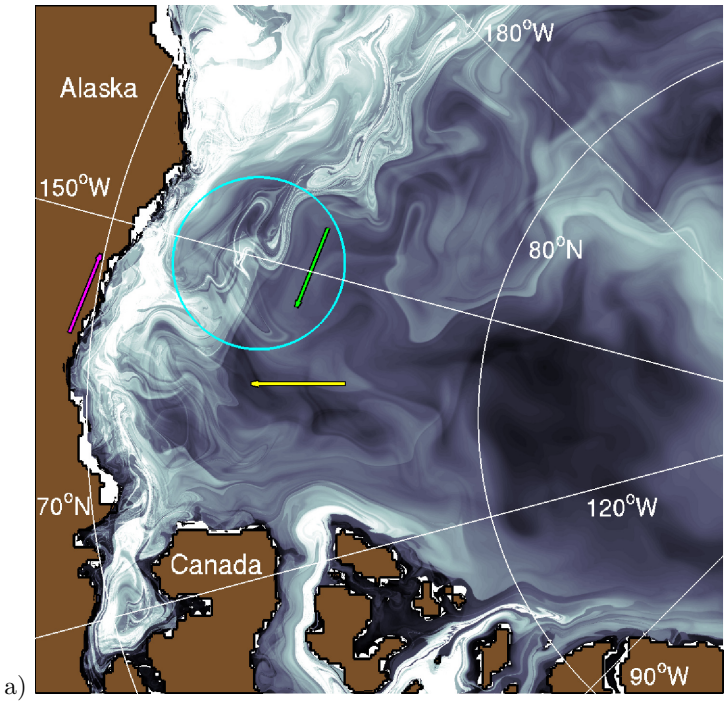

a)

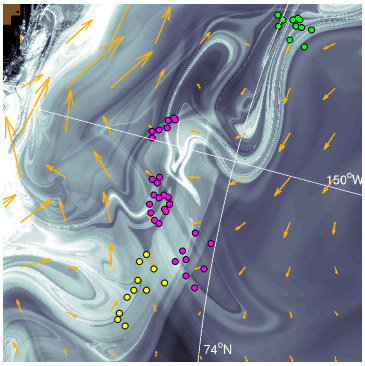

b) 1st April 2013

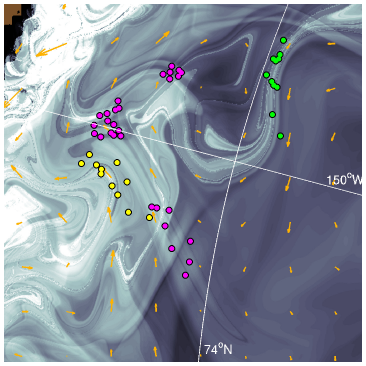

c) 1st June 2013

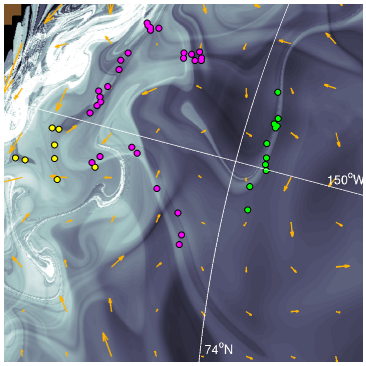

d) 1st August 2013

Figure 11. a) Global view of the Lagrangian structures arising over the Beaufort Sea area on the 1st of April 2013 at 30 m depth, which are identified by the sharp changes in the values of M (evaluated for $\tau = 300$ days). The green, yellow and magenta arrows denote transport directions of the fluid flow meanwhile the cyan circle indicates an area of mixing (highlighted in the following panels) whose dynamics is subjected to these transport directions. Panels b), c) and d) show evolution along a 4 months period of sets of water particles located at the Beaufort Sea. These are depicted in different colors according to the arrows in panel a), that denote directions of the fluid parcels evolution. At the initial date b) these were located at distinct sharp structures generated by the M function. The evolution of these particles is depicted over the representation of the M function computed with $\tau = 300$ days.

We next discuss briefly the suitability of the 2D approach in the context of the transport issues summarized in Figure 11. The vertical curtain like structures of the manifolds in the interior part of the Beaufort Gyre is evidenced by patterns displayed in Fig. 12. This figure shows the manifold geometry at 50m and 100m depths, on the same date as those displayed in figure 11a), confirming the persistence of the major structures, which vary with the vertical coordinate but are not destroyed by the vertical motions.

We end our discussion on transport by focusing on the Transpolar Drift. According to the values that the function M takes over the central Arctic Ocean, highlighted in Fig. 13, we can establish the existence of a permanent jet, the TDS, crossing the region transversally. This is also confirmed in the movie S1. As pointed out in section 2.2, higher M values indicate sea areas where fluid particles move faster. Lower M values are represented in dark gray. Movie S1 confirms that the intensities of the currents become lower in winter and spring time, which are seasons characterized by the thickest sea ice. The thick ice cover shields the ocean from the atmospheric momentum flux, which yields a decay in the velocity of fluid particles. Therefore, the function M takes lower values when evaluated over these seasons, and we observe variations in the intensity of these jets throughout a one-year period. Visible also from M in the movie is the main branch of the TDS and other jets coming from the Siberian coast. In particular the movie shows that from December 2013 onwards, the TDS is fed also by a current branch bringing waters from the Laptev Sea. This is a normal circulation feature in the Arctic for a year of positive AO like 2013 (See http://www.cpc.ncep.noaa.gov/).

Fig. 13 shows the evaluation of M in the central Arctic at four specific dates, starting the 15th April 2013 and ending the 15th of January 2015. The second row shows the results for $\tau = 100$ days and the third row for $\tau = 300$ days. The shorter integration period ($\tau = 100$ days) highlights the structure of the jet forming the Transpolar Drift current. At longer integration periods ($\tau = 300$ days) these features dilute, reflecting that their barrier character weakens in time. The first row

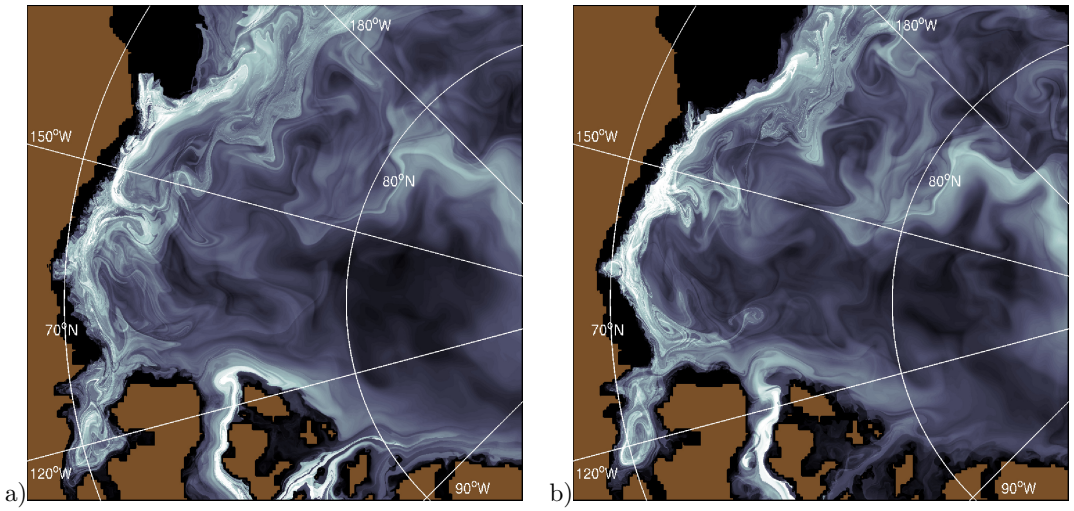

Figure 12. Global view of the Lagrangian structures arising over the Beaufort Sea area on the 1st of April 2013 a) at 50 m depth; b) at 100 m depth. The Lagrangian geometry is identified by the sharp changes in the values of M (evaluated for $\tau = 300$ days).

in Fig. 13 shows the salinity concentration for the corresponding dates. A noticeable feature in these panels is the presence of a strong salinity gradient, visible in greenish color as a transition between yellowish and bluish colours. For instance, in the panel corresponding to column a) this transition is placed approximately between meridians 180^{o}W-150^{o}E; in panel b) the front is more distorted but also remains in that sector; in the panel of the column c), the part of the front closer to north pole, shifts towards the sector between meridians 144^{o}E-108^{o}E; finally in the panel of the column d) the front forms an arch which approximately passes through sectors between meridians 180^{o}W-150^{o}E, 144^{o}E-108^{o}E and 108^{o}E-72^{o}E. The second row makes visible the TDS through the whiter colours in the M function, as previously explained in Figure 6. The TDS is apparent as a jets, which act as barriers of different nature than invariant manifolds, since they are not associated to any hyperbolic trajectory. Recent work by Curbelo et al. (2018a), in the context of the Stratospheric Polar Vortex (SPV), who present similar jet-like features as the ones under discussion, have introduced a heuristic procedure to determine from the M function the boundaries of the SPV, acting as limits of the jet barrier, and have linked those results to the ergodic partition theory (Lopesino et al. 2017; Mezic and Wiggins 1999). Curbelo et al. (2018b) have applied the methodology to determine the boundaries of the SPV on ERA Interim reanalysis. Similar work in this direction has been that by Smith and McDonald (2014). The application of these methods in our context although feasible is beyond the scope of our work. For us it is sufficient to notice that the TDS appears as a jet with a certain width or thickness which has a boundary and that this boundary is close to the transition between light gray and dark tones. In column a) the boundary or limit of the jet is in the sector between meridians 180^{o}W-150^{o}E, as is the salinity barrier in the upper row. Similar correlations are observed in columns b) and d). This correlation is more unclear in column c). The correlations confirm that that the TDS acts as a barrier which prevents the entrance of saltier Atlantic waters into the Canadian basin. The barrier character of the Transpolar Drift is further examined in the third row of Fig. 13. Two particle blobs are placed on both sides of the TDS on the 15th April 2013. Their evolution is displayed in this row through panels a) to d). Panel b) confirms that blobs continue separated on the 15th November 2013, seven months later. Panels c) and d) show that after more than one year, waters at both sides of the Transpolar Drift are eventually at the same side. These findings are consistent with the weakening of the jet features displayed by M at longer integrations periods, and with observations. Figure 14 show the evolution of the temperature and salinity averages within each blob for almost two years. The time series exhibit intermittent jumps caused by the assimilation updates, probably related to assimilation of sea ice concentrations, which increments seem to have zero average. They are restricted both temporally to the Summer 2013 and regionally to the Eastern Transpolar Drift waters and could be caused by the lack of representation of melt ponds in the TOPAZ4 model, although those affect significantly the retrievals of assimilated ice concentrations. The EnKF assimilation is not used with vertical localization and such biases can therefore be passed downwards from the sea ice to the ocean variables. The temperatures follow a weak seasonal cycle of about 0.2 deg, less pronounced in the Eastern Transpolar Drift waters due to the higher ice coverage and thicker ice shelter. The salinities increase during the period January to May 2014 due to brine rejection, then decrease slightly during the following melt season. After the second summer, the temperatures become the same in both blobs but the salinities keep an offset of about 0.4 psu with Eastern waters fresher than Western waters. The water masses had almost identical properties in the Fall 2013 but differences of ice coverage and mixing with neighbouring water masses, both lateral and vertical, have accentuated their differences. The blobs do not homogenize their salinity since the western waters circulate clockwise towards the south of the Canadian basin, where more salty waters are found.

4. Conclusions and outlook

This article examines transport processes in the Arctic circulation by analyzing from a dynamical systems perspective velocity fields produced by CMEMS on a daily basis. Our goal is to examine the horizontal mixing of water masses within the Arctic cold halocline, supported by 2D Lagrangian geometrical structures which verify a 3D layered structure. Our Lagrangian analysis output comprises a period from March 2013 to March 2015 and focuses on two classical Arctic features: the Beaufort Gyre and the Transpolar Drift.

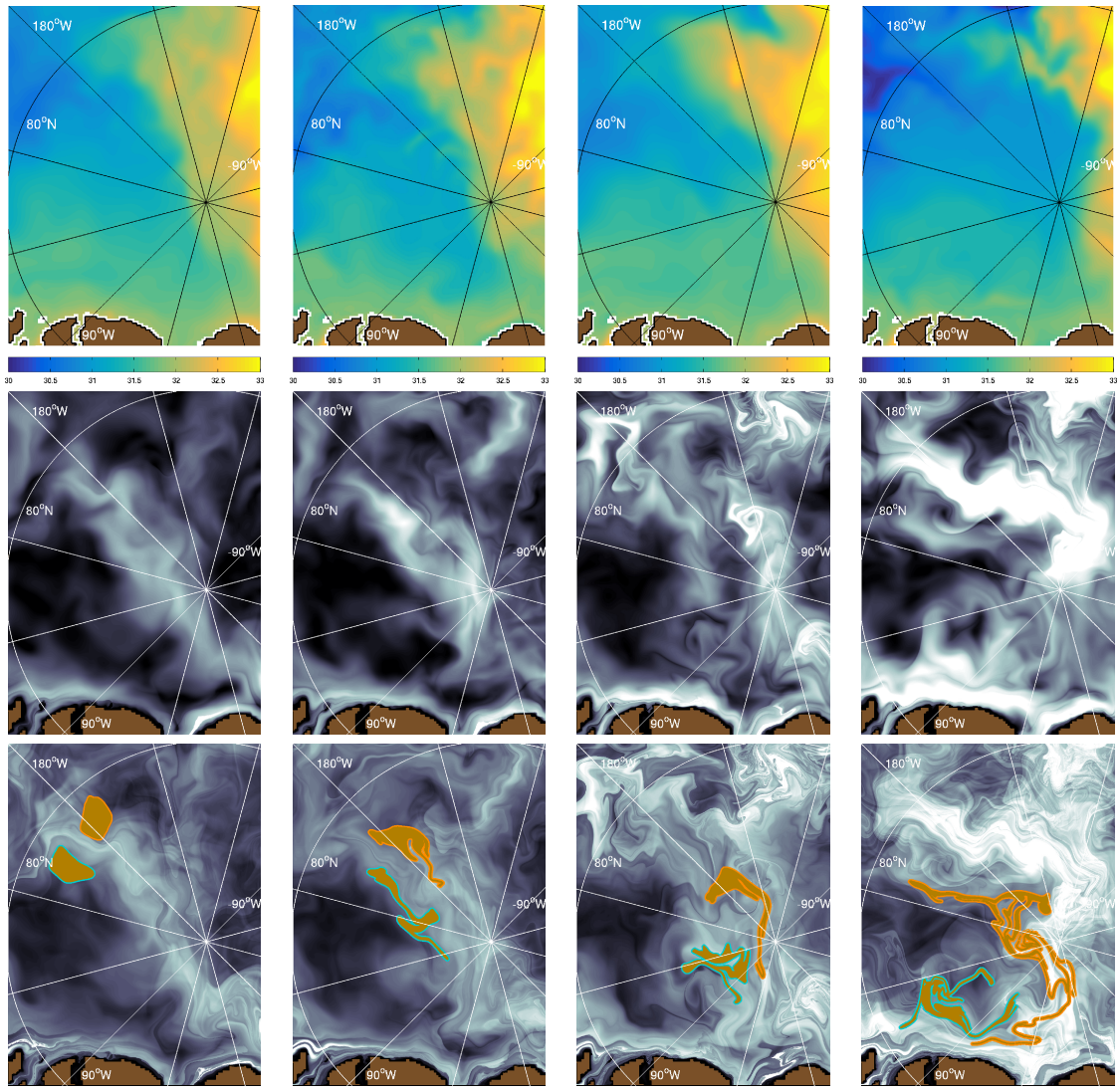

Figure 13. In the upper row panels represent salinity (in parts per thousand) on different dates running from 15th April 2013 (column (a)), 15th November 2013 (column (b)), 15th June 2014 (column (c)), to 15th January 2015 (column (d)). The colorbar varies from 30 to 33 psu of salt in water. The second and third rows represent the function M calculated respectively with $\tau = 100$ and $\tau = 300$ days. The lower row includes two blobs of water particles depicted in brown at both sides of the Transpolar Drift Stream which are advected throughout the panels.

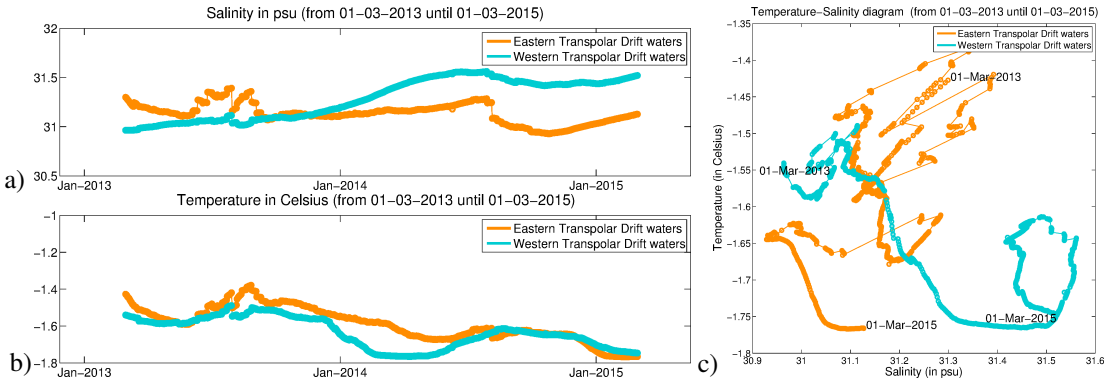

Figure 14. Evolution of averaged properties in the blobs placed at both sides of the Transpolar Drift (see Figure 13). a) Evolution of the salinity average within each blob; b) evolution of the temperature average within each blob; c) Temperature-Salinity diagram for the time series displayed in panels a) and b).

The Lagrangian tool used in this study is the Lagrangian descriptor function M. This tool detects the Lagrangian structures such as hyperbolic trajectories and their stable and unstable manifolds. In the Beaufort Gyre area the function M reveals the presence of a hyperbolic trajectory placed near the North American coast in a detachment configuration. The hyperbolic point is a moving saddle with a stable manifold aligned with the coast and an unstable manifold transversal to it, which acts as a barrier preventing saltier Chukchi Sea waters from mixing with fresher Beaufort Gyre waters. Long

term transport analysis confirms clockwise transport in the interior of the Beaufort Gyre mediated by stable and unstable manifolds of this hyperbolic region.

The presence of a hyperbolic region in a detachment configuration provides a simple skeleton of the transport in the Beaufort Gyre, that may provide interesting insights on more practical issues that recently have drawn much attention, such as the potential impact of oil spills in the Beaufort Sea (Report 2014). These aspects are now under scrutiny, since the reduced ice cover in the Arctic is making this region more attractive to offshore activities such as oil and gas exploration. One particular region of potential interest for this type of exploitation is the continental shelf off the Mackenzie delta. The results discussed in this article suggest that spills occurring along this shore, would evolve in time by contracting themselves while approaching the detachment point according to the dynamics imposed by the stable manifold. Once in the neighborhood of the saddle point, an oil spill would evolve following the unstable manifold, either by turning back to the coast consistently with one of the unstable branches or by moving far into the Beaufort Sea through the other unstable branch. The moving saddle thus marks the position of a highly dispersive region, which elongates the material of potential accidents, pushing it towards the interior of the Arctic, i. e., towards inaccessible regions in the winter period, that would make support for oil spill remediation very complicated during several months. A recent article by García-Garrido et al. (2016) confirms the usefulness of this dynamical systems perspective to describe real oil-spill events.

Finally our Lagrangian tools have revealed the Transpolar Drift as a jet-like dynamical barrier preventing Atlantic waters from invading the Canadian basin and supporting a strong salinity gradient in the area. Our analysis shows that this dynamic feature may hold waters unmixed for periods of up to two years. Additionally our methodology illustrates the variability of the TDS intensity throughout the analyzed period and identifies secondary currents feeding the TDS.

Acknowledgements

F. Balibrea-Iniesta, V. J. García-Garrido and A. M. Mancho are supported by MINECO grants MTM2014-56392-R and SEV-2011-0087 and ONR grant N00014-17-1-3003. They thank to CESGA and ICMAT for computing facilities. F. Balibrea-Iniesta and A. M. Mancho acknowledge a STSM at NERSC funded by ESSEM COST Action ES1402. L. Bertino and J. Xie acknowledge grants of CPU time and data storage from the Norwegian supercomputing project Sigma2 with numbers nn2993k and ns2993k. The research of S. Wiggins is supported by ONR grant No. N00014- 01-1-0769. This paper is a contribution to the Bjerknes Center for Climate Research. We would like to thank Annette Samuelsen for fruitful discussions.

References

Aagaard, K. and Carmack, E. C. (1989). The role of sea ice and other fresh water in the Arctic circulation. *Journal of Geophysical Research*, 94(c10):14485–14498.

Aref, H. (1984). Stirring by chaotic advection. *J. Fluid Mech.*, 143:1–21.

Aurell, E., Boffeta, G., Crisanti, A., Paladin, G., and Vulpiani, A. (1997). Predictability in the large: An extension of the concept of Lyapunov exponent. *J. Phys. A: Math. Gen.*, 30:1–26.

Bleck, R. (2002). An oceanic general circulation model framed in hybrid isopycnic-cartesian coordinates. *Ocean Modelling*, 37:55–88.

Branicki, M. and Kirwan Jr., A. D. (2010). Stirring: The eckart paradigm revisited. *Int. J. Eng. Sci*, 48:1027–1042.

Branicki, M., Mancho, A. M., and Wiggins, S. (2011). A Lagrangian description of transport associated with a Front-Eddy interaction: application to data from the North-Western Mediterranean Sea. *Physica D*, 240(3):282–304.

Carmack, E. C., Yamamoto-Kawai, M., Haine, T. W., Bacon, S., Bluhm, B. A., Lique, C., Melling, H., Polyakov, I. V., Straneo, F., Timmermans, M. L., and Williams, W. J. (2016). Freshwater and its role in the Arctic Marine System: Sources, disposition, storage, export, and physical and biogeochemical consequences in the Arctic and global oceans. *Journal of Geophysical Research G: Biogeosciences*, 121(3):675–717.

Cohen, J., Screen, J. A., Furtado, J. C., Barlow, M., Whittleston, D., Coumou, D., Francis, J., Dethloff, K., Entekhabi, D., Overland, J., and Jones, J. (2014). Recent Arctic amplification and extreme mid-latitude weather. *Nature Geoscience*, 7:627–637.

Curbelo, J., García-Garrido, V. J., Mechoso, C. R., Mancho, A. M., Wiggins, S., and Niang, C. (2017). Insights into the three-dimensional lagrangian geometry of the antarctic polar vortex. *Nonlin. Proc. Geophys.*, 24:379–392.

Curbelo, J., Mechoso, C. R., Mancho, A. M., and Wiggins, S. (2018a). Lagrangian study of the final warming in the southern stratosphere during 2002: Part i. the vortex splitting at upper levels. *Preprint.*

Curbelo, J., Mechoso, C. R., Mancho, A. M., and Wiggins, S. (2018b). Lagrangian study of the final warming in the southern stratosphere during 2002: Part ii. 3d structure. *Preprint.*

de la Cámara, A., Mechoso, C. R., Ide, K., Walterscheid, R., and Schubert, G. (2009). Polar night vortex breakdown and large-scale stirring in the southern stratosphere. *Climate Dynamics*, 35:965–975.

de la Cámara, A., Mechoso, C. R., Serrano, E., and Ide, K. (2013). Quasi-horizontal transport within the Antarctic polar night vortex: Rossby wave breaking evidence and Lagrangian structures. *J. Atmos. Sci.*, 70:2982–3001.

Dee, D. P., Uppala, S. M., Simmons, a. J., Berrisford, P., Poli, P., Kobayashi, S., Andrae, U., Balmaseda, M. a., Balsamo, G., Bauer, P., Bechtold, P., Beljaars, a. C. M., van de Berg, L., Bidlot, J., Bormann, N., Delsol, C., Dragani, R., Fuentes, M., Geer, a. J., Haimberger, L., Healy, S. B., Hersbach, H., Hólm, E. V., Isaksen, L., Kållberg, P., Köhler, M., Matricardi, M., Mcnally, a. P., Monge-Sanz, B. M., Morcrette, J. J., Park, B. K., Peubey, C., de Rosnay, P., Tavolato, C., Thépaut, J. N., and Vitart, F. (2011). The ERA-Interim reanalysis: Configuration and performance of the data assimilation system. *Quarterly Journal of the Royal Meteorological Society*, 137(656):553–597.

Dmitrenko, I. A., Kirillov, S. A., Forest, A., Gratton, Y., Volkov, D. L., Williams, W. J., Lukovich, J. V., Belanger, C., and Barber, D. G. (2016). Shelfbreak current over the Canadian Beaufort Sea continental slope: Wind-driven events in January 2005. *Journal of Geophysical Research : Oceans*, 121:2447–2468.

d'Ovidio, F., Fernández, V. Hernández-García, E., and López, C. (2004). Mixing structures in the mediterranean sea from finite-size lyapunov exponents. *Geophys. Res. Lett.*, 31(17):L17203.

Evensen, G. (2003). The Ensemble Kalman Filter: theoretical formulation and practical implementation. *Ocean Dynamics*, 53(4):343–367.

García-Garrido, V. J., Ramos, A., Mancho, A. M., Coca, J., and Wiggins, S. (2016). A dynamical systems perspective for a real-time response to a marine oil spill. *Marine Pollution Bulletin*, 112:201–210.

Giles, K. A., Laxon, S. W., Ridout, A. L., Wingham, D. J., and Bacon, S. (2012). Western arctic ocean freshwater storage increased by wind-driven spin-up of the beaufort gyre. *Nature Geoscience*, 194-197.

Holloway, G., Nguyen, A., and Wang, Z. (2011). Oceans and ocean models as seen by current meters. *Journal of Geophysical Research*, 116(June):C00D08.

Hunke, E. C. and Dukowicz, J. K. (1997). An elastic-viscous-plastic model for sea ice dynamics. *Journal of Physical Oceanography*, 27:1849–1867.

Ide, K., Small, D., and Wiggins, S. (2002). Distinguished hyperbolic trajectories in time dependent fluid flows: analytical and computational approach for velocity fields defined as data sets. *Nonlin. Proc. Geophys.*, 9:237–263.

Jones, C. K. R. T. and Winkler, S. (2002). Invariant manifolds and Lagrangian dynamics in the ocean and atmosphere. In *Handbook of dynamical systems*, pages 55–92. North-Holland, Amsterdam.

Ju, N., Small, D., and Wiggins, S. (2003). Existence and computation of hyperbolic trajectories of aperiodically time-dependent vector fields and their approximations. *Int. J. Bif. Chaos*, 13:1449–1457.

Krishfield, R. A., Proshutinsky, A., Tateyama, K., Williams, W. J., Carmack, E. C., McLaughlin, F. A., and Timmermans, M.-L. (2014). Deterioration of perennial sea ice in the Beaufort Gyre from 2003 to 2012 and its impact on the oceanic freshwater cycle. *Journal of Geophysical Research*, 119:1271–1305.

L.A., M. (2001). Patterns of Arctic circulation. *Science*, 293:1269–1270.

Large, W. G., McWilliams, J. C., and Doney, S. C. (1994). Oceanic vertical mixing: A review and a model with a nonlocal boundary layer parameterization. *Reviews of Geophysics*, 32(4):363.

Lin, P., Pickart, R. S., Moore, G. W. K., Spall, M. A., and Jianyu, H. (2017). Characteristics and dynamics of wind-driven upwelling in the Alaskan Beaufort Sea based on six years of mooring data. *Deep-Sea Research II*, (submitted).

Lopesino, C., Balibrea-Iniesta, F., García-Garrido, V. J., Wiggins, S., and Mancho, A. M. (2017). A theoretical framework for lagrangian descriptors. *International Journal of Bifurcation and Chaos*, 27:1730001.

M., N. J. (1989). Quantifying local predictability in phase space. *Physica D*, 35(237-250).

Madrid, J. A. J. and Mancho, A. M. (2009). Distinguished trajectories in time dependent vector fields. *Chaos*, 19:013111.

Mancho, A. M., Small, D., and Wiggins, S. (2004). Computation of hyperbolic and their stable and unstable manifolds for oceanographic flows represented as data sets. *Nonlin. Proc. Geophys.*, 11:17–33.

Mancho, A. M., Small, D., and Wiggins, S. (2006). A tutorial on dynamical systems concepts applied to Lagrangian transport in oceanic flows defined as finite time data sets: Theoretical and computational issues. *Phys. Rep.*, 237(3-4).

Mancho, A. M., Wiggins, S., Curbelo, J., and Mendoza, C. (2013). Lagrangian Descriptors: A Method for Revealing Phase Space Structures of General Time Dependent Dynamical Systems. *Communications in Nonlinear Science and Numerical Simulation*, 18:3530–3557.

Melsom, A., Bertino, L., and Sutherland, G. (2015). Quality information document for the Arctic ocean physical analysis and forecast product ARCTIC_ANALYSIS_FORECAST_PHYS_002_001_A. Available at: http://marine.copernicus.eu/documents/QUID/CMEMS-ARC-QUID-002-001a.pdf.

Mendoza, C. and Mancho, A. M. (2010). The hidden geometry of ocean flows. *Phys. Rev. Lett.*, 105(3):038501.

Mendoza, C. and Mancho, A. M. (2012). The Lagrangian description of ocean flows: a case study of the Kuroshio current. *Nonlin. Proc. Geophys.*, 19(4):449–472.

Mendoza, C., Mancho, A. M., and Wiggins, S. (2014). Lagrangian Descriptors and the Assesment of the Predictive Capacity of Oceanic Data Sets. *Nonlin. Proc. Geophys.*, 21:677–689.

Mezic, I. and Wiggins, S. (1994). On the integrability and perturbation of three-dimensional fluid flows with symmetry. *J. Nonlinear Sci.*, 4:157–194.

Mezic, I. and Wiggins, S. (1999). A method for visualization of invariant sets of dynamical systems based on the ergodic partition. *Chaos*, 9(1):213–218.

Morison, J., Kwok, R., Peralta-Ferriz, C., Alkire, M., Rigor, I., Andersen, R., and Steele, M. (2012). Changing arctic ocean freshwater pathways. *Nature*, 481:66–70.

Oki, T. and Sud, Y. C. (1998). Design of the global river channel network for Total Runoff Integrating Pathways (TRIP). *Earth Interactions*, 2(2-001):1–37.

Ottino, J. M. (1989). *The Kinematics of Mixing: Stretching, Chaos, and Transport*. Cambridge University Press, Cambridge, England. Reprinted 2004.

Ottino, J. M. (1990). Mixing, chaotic advection and turbulence. *Annu. Rev. Fluid Mech.*, 22:207–253.

Panteleev, G., Nechaev, D. A., Proshutinsky, A., Woodgate, R., and Zhang, J. (2010). Reconstruction and analysis of the Chukchi Sea circulation in 1990-1991. *Journal of Geophysical Research: Oceans*, 115(8):1–22.

Peralta-Ferriz, C. and Woodgate, R. A. (2015). Seasonal and interannual variability of pan-Arctic surface mixed layer properties from 1979 to 2012 from hydrographic data, and the dominance of stratification for multiyear mixed layer depth shoaling. *Progress in Oceanography*, 134:19–53.

Pickart, R. S., Nobre, C., Lin, P., Arrigo, K. R., Ashjian, C. J., Berchok, C., Cooper, L. W., M., G. J., Hartwell, I., He, J., Itoh, M., Kikuchi, T., Nishino, S., and Vagle, S. (2017). Seasonal to Mesoscale Variability of Water Masses and Atmospheric Conditions in Barrow Canyon, Chukchi Sea. *Deep-Sea Research II*, (submitted).

Polyakov, I. V., Pnyushkov, A. V., Alkire, M. B., Ashik, I. M., Baumann, T. M., Carmack, E. C., Goszczko, I., Guthrie, J., Ivanov, V. V., Kanzow, T., Krishfield, R., Kwok, R., Sundfjord, A., Morison, J., Rember, R., and Yulin, A. (2017). Greater role for Atlantic inflows on sea-ice loss in the Eurasian Basin of the Arctic Ocean. *Science*, 356(6335):285–291.

Proshutinsky, A., Krishfield, R., Timmermans, M.-L., Toole, J., Carmack, E., McLaughlin, F., Williams, W. J., Zimmermann, S., Itoh, M., and Shimada, K. (2009). Beaufort Gyre freshwater reservoir: State and variability from observations. *Journal of Geophysical Research*, 114:C00A10.

Rampal, P., Weiss, J., Dubois, C., and Campin, J.-M. (2011). IPCC climate models do not capture Arctic sea ice drift acceleration: Consequences in terms of projected sea ice thinning and decline. *Journal of Geophysical Research*, 116:C00D07.

Report, W. W. L. F. S. (2014). *Modeling Oil Spills in the Beaufort Sea*. http://awsassets.wwf.ca/downloads/wwf_beaufort_sea_oil_spill_modelling_summ

Sakov, P., Counillon, F., Bertino, L., Lisæter, K. A., Oke, P. R., and Korablev, A. (2012). TOPAZ4: an ocean-sea ice data assimilation system for the North Atlantic and Arctic. *Ocean Science*, 8(4):633–656.

Samelson, R. and Wiggins, S. (2006). *Lagrangian Transport in Geophysical Jets and Waves: The Dynamical Systems Approach*. Springer-Verlag, New York.

Shadden, S. C., Lekien, F., and Marsden, J. E. (2005). Definition and properties of Lagrangian Coherent structures from finite-time Lyapunov exponents in two-dimensional aperiodic flows. *Physica D*, 212:271–304.

Smale, S. (1967). Differentiable dynamical systems. *Bull. Amer. Math. Soc.*, 73((1)):39–44.

Smale, S. (1980). *The Mathematics of Time: Essays on Dynamical Systems, Economic Processes and Related Topics*. Springer Verlag, NY.

Smith, M. L. and McDonald, A. J. (2014). A quantitative measure of polar vortex strength using the function M. *Journal of Geophysical Research Atmos*, 119:5996–5985.

Spall, M. A. (2007). Circulation and water mass transformation in a model of the Chukchi Sea. *Journal of Geophysical Research*, 112:C05025.

Timmermans, M. L., Proshutinsky, A., Krishfield, R. A., Perovich, D. K., Richter-Menge, J. A., Stanton, T. P., and Toole, J. M. (2011). Surface freshening in the Arctic Ocean's Eurasian Basin: An apparent consequence of recent change in the wind-driven circulation. *Journal of Geophysical Research: Oceans*, 116(7):1–17.

Tsubouchi, T., Bacon, S., Aksenov, Y., Garabato, A. C. N., Curry, B., and Lee, C. M. (2017). The Arctic Ocean seasonal cycles of heat and freshwater fluxes : observation- based inverse estimates. *Journal of Physical Oceanography*, (Submitted).

Uotila, P., Goosse, H., Haines, K., Chevallier, M., Barthélemy, A., Bricaud, C., Carton, J., Fučkar, N., Garric, G., Iovino, D., Kauker, F., Korhonen, M., Lien, V. S., Marnela, M., Massonnet, F., Mignac, D., Peterson, K. A., Sadikni, R., Shi, L., Tietsche, S., Toyoda, T., Xie, J., and Zhang, Z. (2018). An assessment of ten ocean reanalyses in the polar regions. *Climate Dynamics*, pages 1–38.

Watanabe, E. (2011). Beaufort shelf break eddies and shelf-basin exchange of Pacific summer water in the western Arctic Ocean detected by satellite and modeling analyses. *Journal of Geophysical Research: Oceans*, 116(8):1–16.

Wiggins, S. (1994). *Normally Hyperbolic Invariant Manifolds in Dynamical Systems*. Applied Mathematical Sciences. Springer.

Wiggins, S. (2005). The dynamical systems approach to Lagrangian transport in oceanic flows. *Annu. Rev. Fluid Mech.*, 37:295–328.

Wiggins, S. and Ottino, J. (2004). Foundations of chaotic mixing. *Phil. Trans. Roy. Soc.*, 362 (1818):937–970.

Woodgate, R. A., Aagaard, K., and Weingartner, T. J. (2005). Monthly temperature, salinity, and transport variability of the Bering Strait through flow. *Geophys. Res. Lett.*, 32.

Xie, J., Bertino, L., Counillon, F., Lisæter, K. A., and Sakov, P. (2017). Quality assessment of the TOPAZ4 reanalysis in the Arctic over the period 1991–2013. *Ocean Science.*, 13.